JACS
JOURNAL OF THE AMERICAN CHEMICAL SOCIETY
pubs.acs.org/JACS
Communication

Open Access
This article is licensed under CC-BY-NC-ND 4.0

Excited Triplet State of Heptacene Studied by Electron Spin Resonance

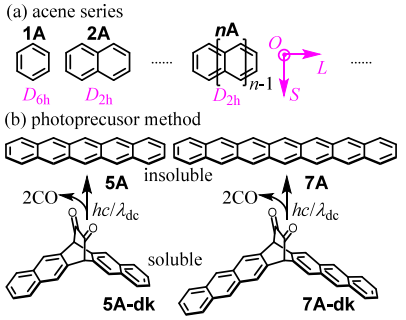
Mikaru Masuda, Joel Hao Jorolan, Hironobu Hayashi, Hiroko Yamada, Tomoaki Miura, and Tadaaki Ikoma*

Cite This: J. Am. Chem. Soc. 2026, 148, 36309−36313
Read Online
ACCESS | Metrics & More | Article Recommendations | Supporting Information

ABSTRACT: Excited triplet states of acene (^{3}***n*A***, *n* being the number of benzene rings) have recently attracted considerable attention because of their useful applications. However, ^{3}***n*A*** with $n > 5$ have not been experimentally explored, due to the insolubility and instability of the higher acenes. In this study, we succeeded in detecting spin-polarized ^{3}**7A*** by combining the photoprecursor method using a degassed amorphous matrix of *o*-terphenyl and time-resolved electron spin resonance. ^{3}**7A*** is the longest acene among the ^{3}***n*A*** observed to date. It has been clarified that ^{3}**7A*** is generated by preferential intersystem crossing to the in-plane sublevels and possesses zero-field splitting constants of $D = 0.035$ cm^{-1} and $E = 0.000$ cm^{-1}. The D values for ^{3}***n*A*** ($n = 2-7$) were found to follow a linear $1/n$-dependence, expressed as $D(n)=0.180/n+0.011$ [cm^{-1}], which provides a quantitative basis for the spatial extent of excitation in even higher ^{3}***n*A*** states.

Acene (***n*A**), in which *n* benzene rings are linearly fused as illustrated in Scheme 1a, is a core molecule in the chemistry of various aromatics[1−3] and is a central building block for organic semiconductors.[4,5]

Scheme 1. (a) Molecular Structure, Molecular Axis System, And Point Group of Acenes (*n*A); (b) Photodecarbonylation Reaction of 5A- and 7A-Diketones (5A-dk and 7A-dk)



Varying *n* allows tuning of the HOMO−LUMO energy gap of ***n*A**.[6,7] Light absorption arising from the narrowed HOMO−LUMO gap enables excited-state chemistry applicable to solar energy utilization, phototherapy, quantum information processing and optoelectronics. Photochemistry often proceeds from the excited triplet state, ^{3}***n*A***, which is typically born from excited singlet state, ^{1}***n*A***, via intersystem crossing (isc), because its lifetime is longer than that of ^{1}***n*A***.[8] Recently ^{3}**5A*** has attracted attention as a molecule exhibiting MASER emission at room temperature,[9,10] a quantum-entanglement state involving many nuclear spin qubits of the hydrogens bonded to carbons.[11−13] ^{3}**5A*** and its derivatives are also utilized as sources of spin angular momentum at room temperature in dynamic nuclear polarization enhancing NMR sensitivity.[14,15] Assemblies of ***n*A** with $n \geq 4$ are expected to undergo singlet fission,[16,17] which may enable surpassing the theoretical limit of solar-energy conversion efficiency.[18,19] Thus, clarifying the electronic structure and dynamics of ^{3}***n*A*** is an urgent and important issue in photochemistry and exciton engineering. In this paper, we performed electron spin resonance (ESR) measurements on ^{3}**7A*** photogenerated from the precursor, **7A-dk** (Scheme 1b), to obtain the magnetic and kinetic properties of the spin-sublevels for higher ^{3}***n*A*** with *n* > 5, for which no experimental studies have been reported to date.

Absorption spectra for **7A-dk** and **5A-dk** in degassed *o*-terphenyl (OTP), whose detailed preparation procedure is described in section S1 of Supporting Information (SI), are shown in Figure 1. When the nπ* band of the dicarbonyl group[20] was excited in the wavelength (λ) range of 400−500 nm using intense light for the decarbonylation (λ_{dc}), the nπ* bands decreased in intensity and several new bands appeared. The light-induced spectrum peaking at λ = 636, 689, 763, and 795 nm for **7A-dk** (Figure 1a), which is almost identical to that for **7A**,[21,22] demonstrates that **7A** is produced from **7A-dk** in OTP at room temperature. Since **7A** exhibits several absorption peaks in the 400−500 nm region, the two peaks at λ = 427 and 452 nm, which overlap with the bleached nπ* band are attributed to **7A**. Additional weak doublet in the 530−600 nm region suggests the formation of byproducts. On the other hand, blue-light irradiation of **5A-dk** induces a

Received: March 24, 2026
Revised: August 16, 2026
Accepted: August 18, 2026
Published: August 24, 2026



ACS Publications
© 2026 The Authors. Published by American Chemical Society

Downloaded from pubs.acs.org/jacsat/article-pdf/148/34/36309/6739027/4/jacs.6c06021.pdf by NATL INST FOR MATLS SCIENCE (NIMS) user on 06 October 2026

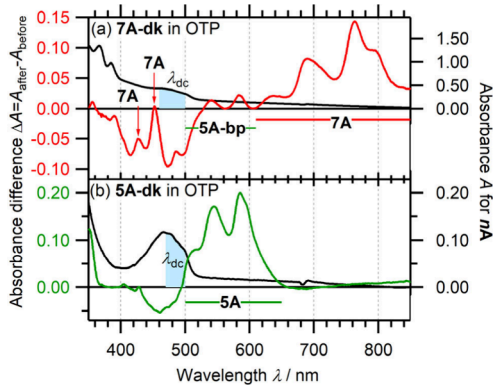


Figure 1. (a) Absorption spectrum (black) for **7A-dk** doped in degassed OTP matrix, and difference spectrum (red) obtained after irradiation with 9 mW light at λ_{dc} = 460−500 nm (light blue) for 39 min at room temperature. The difference spectrum was obtained by subtracting the preirradiation spectrum. (b) Absorption spectrum (black) for **5A-dk** doped in degassed OTP matrix, and difference spectrum (green) after irradiation with 7 mW light at λ_{dc} = 470−500 nm (light blue) for 39 min at room temperature. The spectra recorded before blue-light irradiation (black) exhibit a broad offset due to light scattering.

spectrum with three peaks in the 500−650 nm region (Figure 1b), assigned to **5A**, indicating that **5A** is generated from **5A-dk** by blue-light irradiation at room temperature. The first two peaks in the vibronic progression of absorption spectrum for **5A** in OTP agree with the doublet due to the byproduct of **7A-dk** in OTP. This observation suggests the formation of a byproduct containing a **5A** moiety (**5A-bp**), which is supported by ESR measurements (section S2 of SI). The photogenerated **7A** and **5A** in OTP were stable even under selective photoexcitation (section S3 of SI). We also performed the same experiments using a degassed poly(methyl methacrylate) (PMMA) matrix and observed matrix-dependent photostability of **7A** and **5A** (section S3 of SI).

Figure 2 shows the transient ESR (trESR) spectra for ^{3}**7A*** and ^{3}**5A***, detected at delay time (t) of 1.0 μs after the selective excitation of the photogenerated **7A** and **5A** in degassed OTP at room temperature using the nanosecond lasers. Because the trESR spectrum for ^{3}**7A*** at 80 K has a good signal-to-noise ratio, the spectrum at t = 0.4 μs is also superimposed in Figure 2a. The intensity of ESR signal for ^{3}**7A*** linearly increases with the incident laser power. The observed linear dependence indicates that ^{3}**7A*** is generated by a one-photon process, excluding the possibility of two-photon excitation of **7A-dk** or the byproducts in OTP. Indeed, the total splitting of trESR spectrum of ^{3}**7A*** (ca. 78 mT) is much narrower than that of ^{3}**7A-dk*** (ca. 140 mT), which was detected in OTP at 85 K (Figure S4). Both trESR spectra of ^{3}**7A*** and ^{3}**5A*** exhibit microwave emission on the low field side and absorption on the high field side. The spectral pattern of ^{3}**7A*** resembles those of ^{3}**5A*** and small ^{3}***n*A***. This similarity indicates that the upper spin-sublevels in ^{3}**7A*** are preferentially populated through spin−orbit (SO) interaction with ^{1}**7A***. Although the spectral phase could also be explained by rapid energy transfer from an excited triplet state of nearby molecule with a similar energy,[23] the energy of ^{3}**7A-dk*** (2.36 eV) is much higher than that of ^{3}**7A*** (0.79 eV).[20,24] Therefore, this mechanism of triplet energy transfer can be ruled out for the observed spin polarization of ^{3}**7A***. The spectral width of ^{3}**7A*** is narrower than that of ^{3}**5A***, reflecting the smaller zero-field splitting

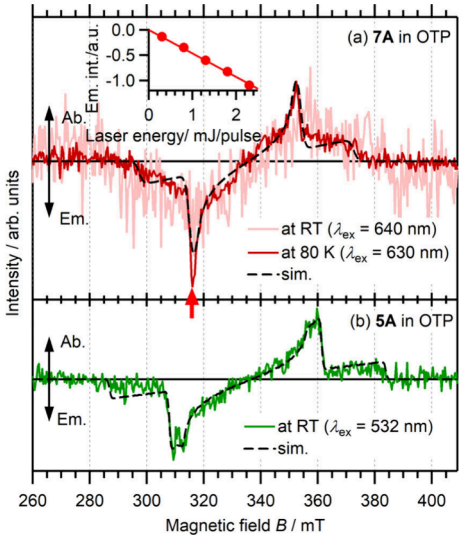


Figure 2. (a) TrESR spectra for ^{3}**7A*** measured at room temperature at t = 1.0 μs (light red) and at 80 K at t = 0.4 μs (red) after the nanosecond laser flashes at λ_{ex} = 640 (0.1 mJ/pulse) and 630 nm (0.4 mJ/pulse), respectively, for the selective excitation of **7A** in degassed OTP, which was prepared by the blue light irradiation at λ_{dc} = 450 nm (125 mW) for 4 min at room temperature. Inset indicates laser power dependence of the ESR signal intensity for ^{3}**7A*** at 80 K measured at the canonical field indicated by the red arrow. (b) TrESR spectrum of ^{3}**5A*** measured at room temperature at t = 1.0 μs (green) after the nanosecond laser excitation at λ_{ex} = 532 nm (0.8 mJ/pulse) for the selective excitation of **5A** in degassed OTP, which was prepared by the blue light irradiation at λ_{dc} = 450 nm (12 mW) for 90 min at room temperature. The black dashed curves represent simulations calculated using the ESR parameters listed in Table 1.

(zfs) among the spin-sublevels of ^{3}**7A***. The observed spectra were successfully simulated using the spin Hamiltonian (section S5 in SI) with the parameters listed in Table 1.

Table 1. g Factor, zfs Constants (D and E), Normalized Population Differences (p_I^0), and Spin−Lattice Relaxation Time (T_1)[a] for ^{3}7A* and ^{3}5A* in a Degassed OTP Matrix

*n*A	g	D/cm^{-1}	E/cm^{-1}	p_L^0:p_S^0:p_O^0[d]	T_1/μs
7A[b]	2.005	0.035	0.0000	(1−0):(0−1):0	0.47
5A[c]	2.002	0.045	−0.0015	0.41:0.59:0.00	1.9

[a]Section S6 in SI. [b]80 K. [c]Room temperature. [d]Assuming that the X-, Y-, and Z-axes are respectively parallel to the L-, S-, and O-axes like small ^{3}***n*A*** and that the smallest sublevel population, p_O^0, is zero.

The energies (ε_I) and splitting constants ($D = -3\varepsilon_O/2$ and $|E/D| = |(\varepsilon_L - \varepsilon_S)/3\varepsilon_O)|$) of the spin-sublevels (T_I^0) at zero-field as well as the population (p_I^0) of T_I^0 for ^{3}**7A*** and ^{3}**5A*** are plotted in Figure 3, together with those of $^3\pi\pi^*$ states of small *n*As.[25−31] The subscript I denotes the quantization axes parallel to the molecular axes (Scheme 1). Both the ε_L and ε_O, corresponding to the sublevels (T_L^0 and T_O^0) whose principal axes are parallel to the long in-plane (L) axis and the out-of-plane (O) axis, respectively approach zero with increasing n. In contrast, ε_S for the T_S^0 whose principal axis lies along the short in-plane (S) axis, remains nearly constant, except for n = 1. The observed trend in ε_I is fully explained by the extension of triplet excitation delocalized over the L-axis, which is the direction of ring condensation. Because the zfs in ^{3}***n*A*** is dominated by the magnetic dipolar interaction between two

Downloaded from pubs.acs.org/jacsat/article-pdf/148/34/36309/6739027/4/jacs.6c06021.pdf by NATL INST FOR MATLS SCIENCE (NIMS) user on 06 October 2026

https://doi.org/10.1021/jacs.6c06021
J. Am. Chem. Soc. 2026, 148, 36309−36313

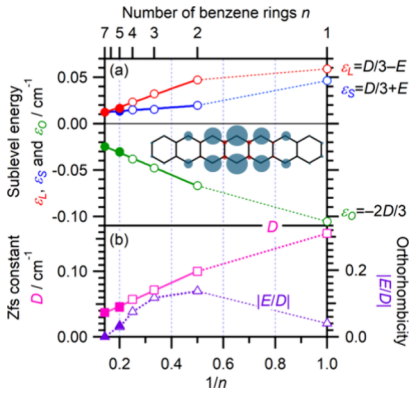


Figure 3. Dependence of the spin-sublevel energy (a) and the D-value and orthorhombicity of zfs (b) on the π-conjugation size. Data of the open symbols are taken from the literatures of **1A**,[25,26] **2A**,[26,27] **3A**,[28,29] **4A**,[31] **5A**,[30] while the filled symbols for **5A** and **7A** represent data obtained in this work. The solid straight lines in (a) and (b) are fitting curves. The inset in (a) shows the spin density distribution for ^{3}**7A*** calculated by DFT.

unpaired electrons in π-orbitals,[32] the ε_J is expressed by eq 1 with the integral of the molecular orbital for triplet excitation, Ψ_T.

$$\varepsilon_J = -\frac{\mu_0}{8\pi}(g\mu_B)^2 \left\langle \Psi_T \left| \frac{r^2 - 3j^2}{r^5} \right| \Psi_T \right\rangle \simeq \frac{\mu_0}{8\pi}(g\mu_B)^2 \sum_{a,b}^{c} \frac{3j_{ab}^2 - r_{ab}^2}{r_{ab}^5} \rho_a \rho_b \quad \{J(j): X(x), Y(y), Z(z)\} \tag{1}$$

Here μ_0, μ_B, r and j denote the permeability, the Bohr magneton, the distance between the unpaired electrons, and the component of r along the J-axis, respectively. The molecular integral can be approximated by a summation of the atomic terms of the spin densities (ρ) on the a- and b-th atoms. In small ^{3}***n*A***, the X-, Y- and Z-axes are assigned to the L-, S- and O-axes, respectively. The decrease of ε_L with n is mainly attributed to increase in the mean value of r caused by the extension of triplet excitation. The decrease of $|\varepsilon_O|$ with n is understood by a reduction in ρ associated with the excitation extension. In contrast, the nearly constant ε_S can be interpreted as the combined effect of two opposing factors, a decrease in ρ and an increase in the number of atomic terms accompanying the excitation extension.

The D-values for ^{3}***n*A*** of n = 2−7 lie well on the line of $D(n) = (0.180 \pm 0.005)/n + (0.011 \pm 0.002)$ [cm^{-1}]. ^{3}**1A*** is excluded from the fitting, because its symmetry is effectively closer to pseudo-D_{6h}.[25,33] A similar dependence of the D-value on the π-conjugation length has been reported for the $^3\pi\pi^*$ states of oligothiophenes[34] and polyenals.[35] The D-value, equal to $-3\varepsilon_O/2$, is proportional to $\langle r^{-3} \rangle$ when Ψ_T is substantially localized into two points, because the O-axis is parallel to the Z-axis, a principal axis with the largest splitting. Therefore, the observed $1/n$-proportionality of D in the $^3\pi\pi^*$ state is likely to arise from the delocalization of triplet excitation. Also, similar linear $1/n$-relationship with a nonzero intercept has also been reported for the HOMO−LUMO gap (E_{gap}) of ^{1}***n*A***.[5,6] As discussed in section S7 in SI, the $1/n$-proportionality of D in ^{3}***n*A*** of n = 2−13 can be understood through the analytical solution derived from a simple model assuming a uniform spin density distribution over the peripheral carbons. To estimate the spin distribution more accurately, we calculated it by the density functional theory (DFT) (section S8 in SI). The calculated distribution can be approximated as Gaussian distributions, whose standard deviations are smaller than the total bond length between the terminal carbon atoms of the two edge rings along the L axis of ***n*A**. Linear $1/n$-proportionalities of the spin-sublevel energies were obtained even in the Gaussian distribution, in which delocalization of excitation is restricted in the central rings (Figure S9).

The preferential isc to the in-plane sublevels observed for ^{3}**7A*** can be explained by the vibronic SO-interaction mediated by $^{1,3}\sigma\pi^*$ (or $^{1,3}\pi\sigma^*$), analogous to the isc mechanism in small ^{3}***n*A*** (section S9 in SI). The g-value of ^{3}**7A***, which is larger than that of the free electron, may also suggest that SO-interaction contributes to the zfs (section S8 in SI).

■ ASSOCIATED CONTENT

Supporting Information

The Supporting Information is available free of charge at https://pubs.acs.org/doi/10.1021/jacs.6c06021.

Experimental details, TrESR spectra of byproducts photogenerated from **7A-dk** in OTP, photoreactivity of diketones and acenes in OTP and PMMA, TrESR spectrum of the T_1 state for **7A-dk** in OTP, simulation of TrESR spectrum, decay kinetics of the T_1 states for **7A** and **5A** in OTP, ring-number Dependence of the D Value, electronic structure and sublevel energies of ^{3}***n*A*** Calculated by DFT, and population rates of ^{3}***n*A*** (PDF)

■ AUTHOR INFORMATION

Corresponding Author

Tadaaki Ikoma − *Graduate School of Science and Technology, Niigata University, Niigata, Niigata 950-2181, Japan; Center for Coordination of Research Facilities, Niigata University, Niigata, Niigata 950-2181, Japan;* orcid.org/0000-0003-2003-6839; Email: ikoma@chem.sc.niigata-u.ac.jp

Authors

Mikaru Masuda − *Graduate School of Science and Technology, Niigata University, Niigata, Niigata 950-2181, Japan*

Joel Hao Jorolan − *Graduate School of Science and Technology, Niigata University, Niigata, Niigata 950-2181, Japan;* Present Address: Western Australia School of Mines, Faculty of Science and Engineering, Curtin University, Kent Street, Bentley, Western Australia 6102, Australia

Hironobu Hayashi − *Center for Basic Research on Materials, National Institute for Materials Science, Tsukuba, Ibaraki 305-0047, Japan;* orcid.org/0000-0002-7872-3052

Hiroko Yamada − *Institute for Chemical Research, Kyoto University, Uji, Kyoto 611-0011, Japan;* orcid.org/0000-0002-2138-5902

Tomoaki Miura − *Graduate School of Science and Technology, Niigata University, Niigata, Niigata 950-2181, Japan;* orcid.org/0000-0002-7281-3049

Complete contact information is available at: https://pubs.acs.org/10.1021/jacs.6c06021

https://doi.org/10.1021/jacs.6c06021
J. Am. Chem. Soc. 2026, 148, 36309−36313

Downloaded from pubs.acs.org/jacsat/article-pdf/148/34/36309/6739027/4/jacs.6c06021.pdf by NATL INST FOR MATLS SCIENCE (NIMS) user on 06 October 2026

Author Contributions

The manuscript was written through contributions of all authors.

Funding

Financial support was provided by JSPS Kakenhi (23K17901) and research grants from Union Tool and TAKEUCHI Scholarship Associations (to T.I.), and JST SPRING JPMJSP2121 (to M.M.).

Notes

The authors declare no competing financial interest.

■ ACKNOWLEDGMENTS

T.I. thanks Prof. Maeda and Prof. Nagashima (Saitama Univ.) for their kind help measuring ESR at QST. M.M. is grateful for a scholarship of SPRING.

■ REFERENCES

(1) Turro, N. J.; Ramamurthy, V.; Scaiano, J. C. *Principles of Molecular Photochemistry, An Introduction*; University Science Books: 2009.
(2) Hepworth, J. D.; Waring, M. J.; Waring, D. R. *Aromatic Chemistry*; The Royal Society of Chemistry: 2002.
(3) Hayashi, H.; Yamada, H. Exploring the chemistry of higher acenes: from synthesis to applications. *Chem. Sci.* **2025**, *16*, 11204−11231.
(4) Pope, M.; Swenberg, C. E. *Electronic Processes in Organic Crystals and Polymers*; 2nd ed.; Oxford University Press: 1999.
(5) Köhler, A.; Bässler, H. *The Electronic Structure of Organic Semiconductors*; Wiley Online Books: 2015.
(6) Shen, B.; Tatchen, J.; Sanchez-Garcia, E.; Bettinger, H. F. Evolution of the Optical Gap in the Acene Series: Undecacene. *Angew. Chem., Int. Ed.* **2018**, *57*, 10506−10509.
(7) Schmitteckert, P.; Thomale, R.; Korytár, R.; Evers, F. Incommensurate quantum-size oscillations in acene-based molecular wires—Effects of quantum fluctuations. *J. Chem. Phys.* **2017**, *146*, 092320.
(8) Turro, N. J.; Ramamurthy, V.; Scaiano, J. C. *Modern Molecular Photochemistry of Organic Molecules*; University Science Books: 2010.
(9) Breeze, J. D.; Salvadori, E.; Sathian, J.; Alford, N. M.; Kay, C. W. M. Continuous-wave room-temperature diamond maser. *Nature* **2018**, *555*, 493−496.
(10) Salvadori, E.; Breeze, J. D.; Tan, K.-J.; Sathian, J.; Richards, B.; Fung, M. W.; Wolfowicz, G.; Oxborrow, M.; Alford, N. M.; Kay, C. W. M. Nanosecond time-resolved characterization of a pentacene-based room-temperature MASER. *Sci. Rep.* **2017**, *7*, 41836.
(11) Kothe, G.; Lukaschek, M.; Yago, T.; Link, G.; Ivanov, K. L.; Lin, T.-S. Initializing 214 Pure 14-Qubit Entangled Nuclear Spin States in a Hyperpolarized Molecular Solid. *J. Phys. Chem. Lett.* **2021**, *12*, 3647−3654.
(12) Madsen, L. S.; Laudenbach, F.; Askarani, M. F.; Rortais, F.; Vincent, T.; Bulmer, J. F. F.; Miatto, F. M.; Neuhaus, L.; Helt, L. G.; Collins, M. J.; Lita, A. E.; Gerrits, T.; Nam, S. W.; Vaidya, V. D.; Menotti, M.; Dhand, I.; Vernon, Z.; Quesada, N.; Lavoie, J. Quantum computational advantage with a programmable photonic processor. *Nature* **2022**, *606*, 75−81.
(13) Wu, Y.; Bao, W.-S.; Cao, S.; Chen, F.; Chen, M.-C.; Chen, X.; Chung, T.-H.; Deng, H.; Du, Y.; Fan, D.; Gong, M.; Guo, C.; Guo, C.; Guo, S.; Han, L.; Hong, L.; Huang, H.-L.; Huo, Y.-H.; Li, L.; Li, N.; Li, S.; Li, Y.; Liang, F.; Lin, C.; Lin, J.; Qian, H.; Qiao, D.; Rong, H.; Su, H.; Sun, L.; Wang, L.; Wang, S.; Wu, D.; Xu, Y.; Yan, K.; Yang, W.; Yang, Y.; Ye, Y.; Yin, J.; Ying, C.; Yu, J.; Zha, C.; Zhang, C.; Zhang, H.; Zhang, K.; Zhang, Y.; Zhao, H.; Zhao, Y.; Zhou, L.; Zhu, Q.; Lu, C.-Y.; Peng, C.-Z.; Zhu, X.; Pan, J.-W. Strong Quantum Computational Advantage Using a Superconducting Quantum Processor. *Phys. Rev. Lett.* **2021**, *127*, 180501.
(14) Tateishi, K.; Negoro, M.; Nishida, S.; Kagawa, A.; Morita, Y.; Kitagawa, M. Room temperature hyperpolarization of nuclear spins in bulk. *Proc. Natl. Acad. Sci. U.S.A.* **2014**, *111*, 7527−7530.
(15) Fujiwara, S.; Hosoyamada, M.; Tateishi, K.; Uesaka, T.; Ideta, K.; Kimizuka, N.; Yanai, N. Dynamic Nuclear Polarization of Metal-Organic Frameworks Using Photoexcited Triplet Electrons. *J. Am. Chem. Soc.* **2018**, *140*, 15606−15610.
(16) Miyata, K.; Conrad-Burton, F. S.; Geyer, F. L.; Zhu, X. Y. Triplet Pair States in Singlet Fission. *Chem. Rev.* **2019**, *119*, 4261−4292.
(17) Suzuki, S.; Sakai, H.; Yamauchi, M.; Hayashi, H.; Mizuhata, Y.; Kato, T.; Hirose, T.; Hasobe, T.; Yamada, H. Observation of Photophysical Processes of a Heptacene Derivative: Monomeric Behavior in Homogeneous Solution and Singlet Fission in Thin Film. *J. Am. Chem. Soc.* **2026**, *148*, 6000−6011.
(18) Li, J.; Cao, H.; Zhang, Z.; Liu, S.; Xia, Y. Research Progress on Singlet Fission in Acenes and Their Derivatives. *Photonics* **2022**, *9*, 689.
(19) Baldacchino, A. J.; Collins, M. I.; Nielsen, M. P.; Schmidt, T. W.; McCamey, D. R.; Tayebjee, M. J. Y. Singlet fission photovoltaics: Progress and promising pathways. *Chem. Phys. Rev.* **2022**, *3*, 021304.
(20) Mondal, R.; Okhrimenko, A. N.; Shah, B. K.; Neckers, D. C. Photodecarbonylation of α-Diketones: A Mechanistic Study of Reactions Leading to Acenes. *J. Phys. Chem. B* **2008**, *112*, 11−15.
(21) Mondal, R.; Shah, B. K.; Neckers, D. C. Photogeneration of Heptacene in a Polymer Matrix. *J. Am. Chem. Soc.* **2006**, *128*, 9612−9613.
(22) Mondal, R.; Tönshoff, C.; Khon, D.; Neckers, D. C.; Bettinger, H. F. Synthesis, Stability, and Photochemistry of Pentacene, Hexacene, and Heptacene: A Matrix Isolation Study. *J. Am. Chem. Soc.* **2009**, *131*, 14281−14289.
(23) Matsumoto, T.; Teki, Y. Theoretical study of dynamic electron-spin-polarization via the doublet-quartet quantum-mixed state (II). Population transfer and magnetic field dependence of the spin polarization. *Phys. Chem. Chem. Phys.* **2012**, *14*, 10178−10186.
(24) Hajgató, B.; Szieberth, D.; Geerlings, P.; De Proft, F.; Deleuze, M. S. A benchmark theoretical study of the electronic ground state and of the singlet-triplet split of benzene and linear acenes. *J. Chem. Phys.* **2009**, *131*, 224321.
(25) de Groot, M. S.; Hesselmann, I. A. M.; van der Waals, J. H. Paramagnetic resonance in phosphorescent aromatic hydrocarbons. *Mol. Phys.* **1969**, *16*, 45−60.
(26) El-Sayed, M. A.; Moomaw, W. R.; Chodak, J. B. The mechanism of the $S_1 \rightsquigarrow T_x$ intersystem crossing process in aromatic hydrocarbons from PMDR. *Chem. Phys. Lett.* **1973**, *20*, 11−16.
(27) Hutchison, C. A.; Mangum, B. W. Paramagnetic Resonance Absorption in Naphthalene in Its Phosphorescent State. *J. Chem. Phys.* **1961**, *34*, 908−922.
(28) Grivet, J. P. Electron Spin Resonance of Phosphorescent Anthracene. *Chem. Phys. Lett.* **1969**, *4* (2), 104−106.
(29) Clarke, R. H.; Hayes, J. M. Triplet state dynamics in polycyclic aromatic molecules. *Chem. Phys. Lett.* **1974**, *27*, 556−561.
(30) Van Strien, A. J.; Schmidt, J. An EPR study of the triplet state of pentacene by electron spin-echo techniques and laser flash excitation. *Chem. Phys. Lett.* **1980**, *70*, 513−517.
(31) Clarke, R. H.; Frank, H. A. Triplet state radiationless transitions in polycyclic hydrocarbons. *J. Chem. Phys.* **1976**, *65*, 39−47.
(32) Loboda, O.; Minaev, B.; Vahtras, O.; Schimmelpfennig, B.; Ågren, H.; Ruud, K.; Jonsson, D. Ab initio calculations of zero-field splitting parameters in linear polyacenes. *Chem. Phys.* **2003**, *286*, 127−137.
(33) Goncalves, A. M. P.; Hutchison, C. A., Jr. Electron Nuclear Double Resonance in Photoexcited Triplet-State Benzene-h6Molecules in Benzene-d6 Single Crystals. *J. Chem. Phys.* **1968**, *49*, 4235−4236.
(34) Bennati, M.; Grupp, A.; Mehring, M.; Bäuerle, P. Pulsed EPR Spectroscopy of the Photoexcited Triplet States of Thiophene Oligomers in Frozen Solution. *J. Phys. Chem.* **1996**, *100*, 2849−2853.

Downloaded from pubs.acs.org/jacsat/article-pdf/148/34/36309/6739274/jacs.6c06021.pdf by NATL INST FOR MATLS SCIENCE (NIMS) user on 06 October 2026

(35) Ros, M.; Groenen, E. J. J. An Electron-Spin Echo Study of the Nonradiative Triplet-State of Polyenals. *J. Chem. Phys.* **1991**, *94*, 7640−7648.

Downloaded from pubs.acs.org/jacsat/article-pdf/148/34/36309/6739027 4/jacs.6c06021.pdf by NATL INST FOR MATLS SCIENCE (NIMS) user on 06 October 2026

https://doi.org/10.1021/jacs.6c06021
J. Am. Chem. Soc. 2026, 148, 36309−36313